Earth and Planetary Science Letters 302 (2011) 448–454

Contents lists available at ScienceDirect

Earth and Planetary Science Letters

journal homepage: www.elsevier.com/locate/epsl

Mantle plumes and associated flow beneath Arabia and East Africa

Sung-Joon Chang *, Suzan Van der Lee

Department of Earth and Planetary Sciences, Northwestern University, 1850 Campus Drive, Evanston, IL 60208-2150, USA

ARTICLE INFO

Article history:
Received 29 April 2010
Received in revised form 25 December 2010
Accepted 28 December 2010
Available online 19 January 2011

Editor: R.W. Carlson

Keywords:
seismic tomography
joint inversion
mantle plume
mantle flow
Arabia
East Africa

ABSTRACT

We investigate mantle plumes and associated flow beneath the lithosphere by imaging the three-dimensional *S*-velocity structure beneath Arabia and East Africa. This image shows elongated vertical and horizontal low-velocity anomalies down to at least mid mantle depths. This three-dimensional *S*-velocity model is obtained through the joint inversion of teleseismic *S*- and *SKS*-arrival times, regional *S*- and Rayleigh waveform fits, fundamental-mode Rayleigh-wave group velocities, and independent Moho constraints from receiver functions, reflection/refraction profiles, and gravity measurements. In the resolved parts of our *S*-velocity model we find that the Afar plume is distinctly separate from the Kenya plume, showing the Afar plume's origin in the lower mantle beneath southwestern Arabia. We identify another quasi-vertical low-velocity anomaly beneath Jordan and northern Arabia which extends into the lower mantle and may be related to volcanism in Jordan, northern Arabia, and possibly southern Turkey. Comparing locations of mantle plumes from the joint inversion with fast axes of shear-wave splitting, we confirm horizontal mantle flow radially away from Afar. Low-velocity channels in our model support southwestward flow beneath Ethiopia, eastward flow beneath the Gulf of Aden, but not northwestwards beneath the entire Red Sea. Instead, northward mantle flow from Afar appears to be channeled beneath Arabia.

1. Introduction

The voluminous Ethiopian flood basalts, widespread Cenozoic volcanism in western Arabia, and anomalous topographic swells have long been attributed to mantle plumes (Camp and Roobol, 1992; Daradich et al., 2003; Ebinger and Sleep, 1998; Schilling, 1973; White and McKenzie, 1989).

Although this region (Fig. 1) has been well studied, there has been no consensus on the number of plumes and associated mantle flow beneath East Africa and Arabia. Ebinger and Sleep (1998) proposed that a single large plume may have caused multiple hotspots via channeled flow along thin lithosphere. This hypothesis has been supported by a number of geophysicists. For example, Ritsema et al. (1999) attribute the extensive volcanism around Afar to mantle flow from the African superplume, which originates at the core–mantle boundary (CMB) beneath South Africa in their global *S*-velocity model. The regional travel time tomographic results of Benoit et al. (2006a,b) support a single plume beneath Ethiopia. Numerical experiments by Daradich et al. (2003) suggest that rift-flank uplift along the Red Sea was induced by the African superplume. On the other hand, numerical mantle convection models of Lin et al. (2005) show that double-plume models can reproduce the distribution of East-African magmatism in space and time. Finite-frequency tomography (Montelli et al., 2004) shows that the Afar plume has a cylindrical, vertical tail through the lower mantle, separate from the African superplume. However, they do not rule out that the Afar plume may merge into the African superplume in the deep lower mantle (Montelli et al., 2006). Shear-wave splitting and tomographic results of Hansen et al. (2006) and Park et al. (2007, 2008) suggest channeled horizontal mantle flow from the Afar hotspot.

On the other hand, several geochemists have proposed the existence of two distinct mantle plumes beneath East Africa. George et al. (1998) used $^{40}Ar/^{39}Ar$ ages to propose distinct mantle plumes beneath Afar and Kenya. Nelson et al. (2007, 2008) and Rogers et al. (2000) also assert two distinct mantle plumes based on Sr, Nd, and Pb isotope evidence. Pik et al. (2006) used He^3/He^4 ratios to suggest that a unique large mantle plume could not feed all the Cenozoic African volcanic provinces. Camp and Roobol (1992) question whether one Afar plume can feed widespread volcanism in western Arabia over a distance of 2000 km, which is twice the radius of a typical plume head (White and McKenzie, 1989). On the contrary, Furman et al. (2006) present geochemical evidence that suggests these different plumes could all stem from a common large mantle plume such as the African superplume.

In summary, current evidence is inconclusive with respect to the following questions. How many mantle plumes exist with different origins beneath East Africa and Arabia? If hot materials are upwelling via those plumes, do they flow along thin lithosphere as a natural

* Corresponding author.
E-mail address: sjchang@earth.northwestern.edu (S.-J. Chang).

0012-821X/$ – see front matter © 2011 Elsevier B.V. All rights reserved.
doi:10.1016/j.epsl.2010.12.050

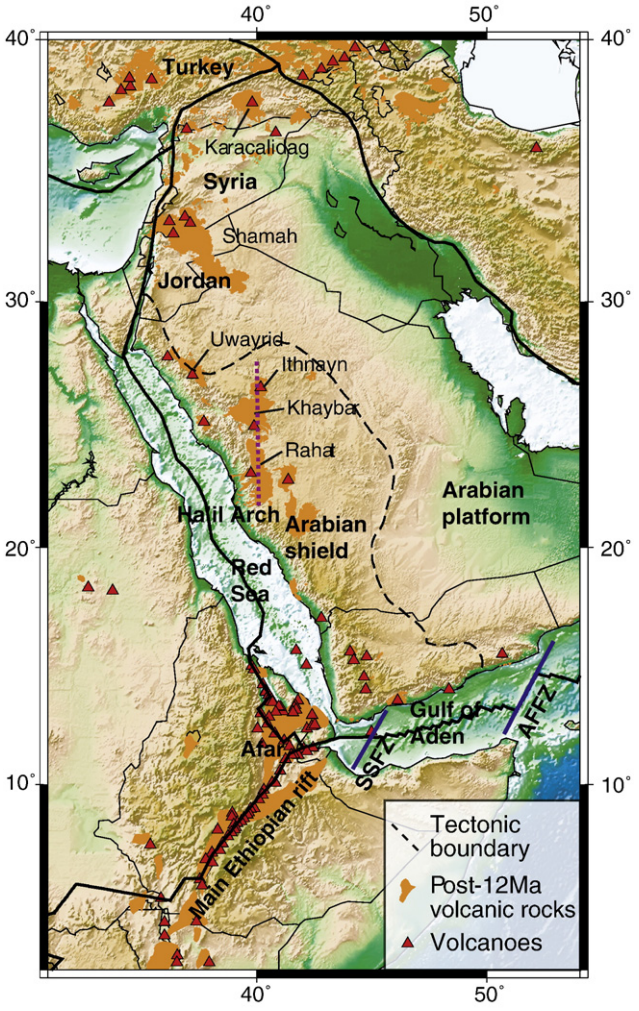

Fig. 1. Topographic map for Arabia and northeastern Africa. Volcanoes and post-12 Ma volcanic rocks are indicated by red triangles and orange area, respectively. Thick solid lines indicate plate boundaries, which are from Bird (2003). A dotted purple line represents the Ha'il Arch. SSFZ: Shukra El Sheik Fracture zone; AFFZ: Alula Fartak Fracture zone.

channel? Can the Afar plume exploit such a channel to cause volcanism as far as Jordan and Turkey? To answer these questions, we jointly invert teleseismic *S*- and *SKS*-arrival times, regional *S*- and Rayleigh waveform fits, fundamental-mode Rayleigh-wave group velocities, and independent Moho constraints to provide complementary resolution for the three-dimensional (3-D) *S*-velocity structure beneath East Africa and Arabia. We demonstrate the unprecedented resolving power of these combined data sets through a series of tests. Our tomographic results help reconcile some of the aforementioned contradictory explanations for the region's volcanism, uplift, and rifting.

2. Method and data

Details on the method and data are given in Chang et al. (2010), but we briefly review them here. Model parameters of *S* velocity are at nodes in a spherical shell at each of 32 different depths, down to 1930 km. The 33rd spherical shell contains model parameters of Moho depth. The shells extend 70° in all directions from the center of our region (35°N/22.5°E). Each spherical shell includes 16,541 nodes roughly 100 km apart at the Earth's surface.

The equation of the joint inversion is as follows

$$\begin{bmatrix} w_{ta}\mathbf{A^{ta}} & w_{ta}\mathbf{A^{ta}_m} & w_{ta}\mathbf{A^{ta}_e} & w_{ta}\mathbf{A^{ta}_o} \\ w_{rw}\mathbf{A^{rw}} & w_{rw}\mathbf{A^{rw}_m} & 0 & 0 \\ w_U\mathbf{A^U} & w_U\mathbf{A^U_m} & 0 & 0 \\ 0 & w_{ic}\mathbf{A^{ic}_m} & 0 & 0 \\ w_1\mathbf{I} & w_1\mathbf{I} & 0 & 0 \\ w_2\mathbf{F_h} & w_2\mathbf{F_h} & 0 & 0 \\ w_3\mathbf{F_v} & 0 & 0 & 0 \end{bmatrix} \begin{bmatrix} \Delta\beta \\ \Delta h \\ \Delta x_e \\ \Delta e \end{bmatrix} = \begin{bmatrix} w_{ta}d^{ta} \\ w_{rw}d^{rw} \\ w_U d^U \\ w_{ic}d^{ic} \\ 0 \\ 0 \\ 0 \end{bmatrix}, \quad (1)$$

where $\mathbf{A^{ta}}$, $\mathbf{A^{rw}}$, $\mathbf{A^U}$, and $\mathbf{A^{ic}}$ are sensitivity matrices to *S* velocity of teleseismic arrival times, regional waveform fits, Rayleigh-wave group velocities, and independent Moho constraints, respectively. The corresponding data vectors are d^{ta}, d^{rw}, d^U, and d^{ic}, respectively. The sensitivity kernels of each data type to Moho depth are represented as $\mathbf{A^{ta}_m}$, $\mathbf{A^{rw}_m}$, $\mathbf{A^U_m}$, and $\mathbf{A}^{ic}_m$, respectively, and the sensitivity kernels to the event location and origin time for teleseismic arrival times are indicated by $\mathbf{A^{ta}_e}$ and $\mathbf{A^{ta}_o}$, respectively. One of several different 1-D reference models is chosen for each path of regional waveforms fits and fundamental-mode group velocities based on average Moho depth and ocean depth for the great-circle path to compute more accurate sensitivity kernels. Model parameters consist of $\Delta\beta$, Δh, Δx_e, and Δe, which are perturbations of *S* velocity, Moho depth, events location, and origin time, respectively. The identity matrix $\mathbf{I}$ serves as the damping operator; $\mathbf{F_h}$ and $\mathbf{F_v}$ are horizontal and vertical flattening operators, respectively. Weights *w* are applied to each data set and operator. The damping operator tends to suppress the effects of data outliers, while the flattening operators avoid rapid non-physical variations of model parameters. Flattening operators are differentials between two laterally or vertically contiguous nodes (Constable et al., 1987; VanDecar, 1991).

Out of a total of about 5600 waveform fits used in the joint inversion, over 3000 waveforms sample the area of interest (Fig. S1a). The frequency content of the waveform fits is generally within the range between 0.006 and 0.1 Hz. Out of all fundamental-mode Rayleigh-wave group-velocity dispersion curves with a period band ranging from 7 to 100 s in the joint inversion, over 5000 dispersion curves sample the study region (Fig. S1b). For relative arrival times, about 3500 teleseismic *S* and 1400 *SKS* phase arrival times are recorded in the study region (Fig. S1c), which are measured with the multi-channel cross-correlation method (VanDecar and Crosson, 1990). We obtained over 40,000 *S* phase arrival times for the study region (Fig. S1c) from the reprocessed ISC database (Engdahl et al., 1998). We incorporated around 400 Moho depth constraints from receiver functions, gravity measurements, refraction, and reflection surveys (Chang et al., 2010; Marone et al., 2003) to avoid mapping crustal structure into mantle structure (Fig. S1d).

3. Resolution tests

We performed several resolution tests to investigate the resolving power of the joint inversion for the study region. First, we test models with vertical cylindrical anomalies of ± 200 m/s, but with different radii of 3° and 1°, as shown in the top panels of Fig. S2. Gaussian random noise is added to synthetic data for the inversion with a standard deviation in proportion to the estimated uncertainty of our data. The cylindrical anomalies with radii of 3° are well resolved beneath Arabia and Ethiopia down to the lower mantle with good amplitude recovery (Fig. S2a). The western boundary of the study region and the Arabian Sea have limited resolution for the whole mantle, but these regions are not of interest in the present paper. Small anomalies with radii of 1° are recovered fairly, with weaker amplitude and some smearing (Fig. S2b), but it is encouraging that